THERMAL-ELASTIC DEFORMATION OF CANDU PRESSURE TUBE FOLLOWING FUEL ELEMENT TO PRESSURE TUBE CONTACT

FARSHAD TALEBI, AZIN BEHDADI, JOHN C. LUXAT

McMaster University, Engineering Physics Department, Hamilton, Ontario, Canada L8S 4L7
e-mail: farshat@mcmaster.ca, behdada@mcmaster.ca, luxatj@mcmaster.ca

ABSTRACT

Thermal strain deformation is a pressure tube failure mechanism. The main objective of this paper is to develop mechanistic models to evaluate local thermal-mechanical deformation of a pressure tube in a CANDU reactor and to investigate fuel channel integrity under localized contact between fuel elements and pressure tube. The consequence of concern is potential creep strain failure of a pressure tube and calandria tube. The initial focus will be on the case where a fuel rod contacts the pressure tube at full power with highly cooling condition. Such an event could occur if a fuel element was to become detached from a bundle. Calculations are performed using the finite element method in which the heat and thermal mechanical strain equations are solved simultaneously. The heat conduction from fuel sheath to the inner surface of the pressure tube with appropriate convective and radiation boundary conditions has been simulated. Furthermore, the thermal-elastic stresses have been obtained for when the pressure tube is under full operational condition. The contact boundary could be a spot or a small arc contact between the fuel sheath and pressure tube. The vapor pockets are considered in the areas beside the contact region where the convective cooling is drastically decreased. Subsequently, modeling has been extended to the contact of number of fuel elements where several fuel rods are postulated to contact the pressure tube under fully cooling conditions. It is observed that the pressure tube thermal strain will occur if sufficiently high temperature is reached. Sensitivity analysis is performed in order to evaluate the contact conductance, the extension of vapor region and the contact width. The pressure tube local strain is very sensitive to these parameters where any local strain will act to reduce the contact width, contact conductance and pressure tube thermal strain and therefore will be self-limiting.

1. INTRODUCTION

The typical CANDU fuel assembly is a 37 rod cluster fuelled with natural uranium oxide and cladded with zircaloy-4 (Figure 1(a)). The fuel assemblies are located inside a pressure tube made of zirconium with 2.5% niobium containing heavy water coolant. This pressure tube is separated by an annular gas-filled insulation gap from the zircaloy-2 calandria tube which is immersed in a heavy water moderator. Normally, the fuel elements (FEs) are not in direct contact with the pressure tube (PT) except at the bearing pads of the outer elements at the bottom of the bundle. Should a sever bundle defect occur, it can be postulated that an element becomes

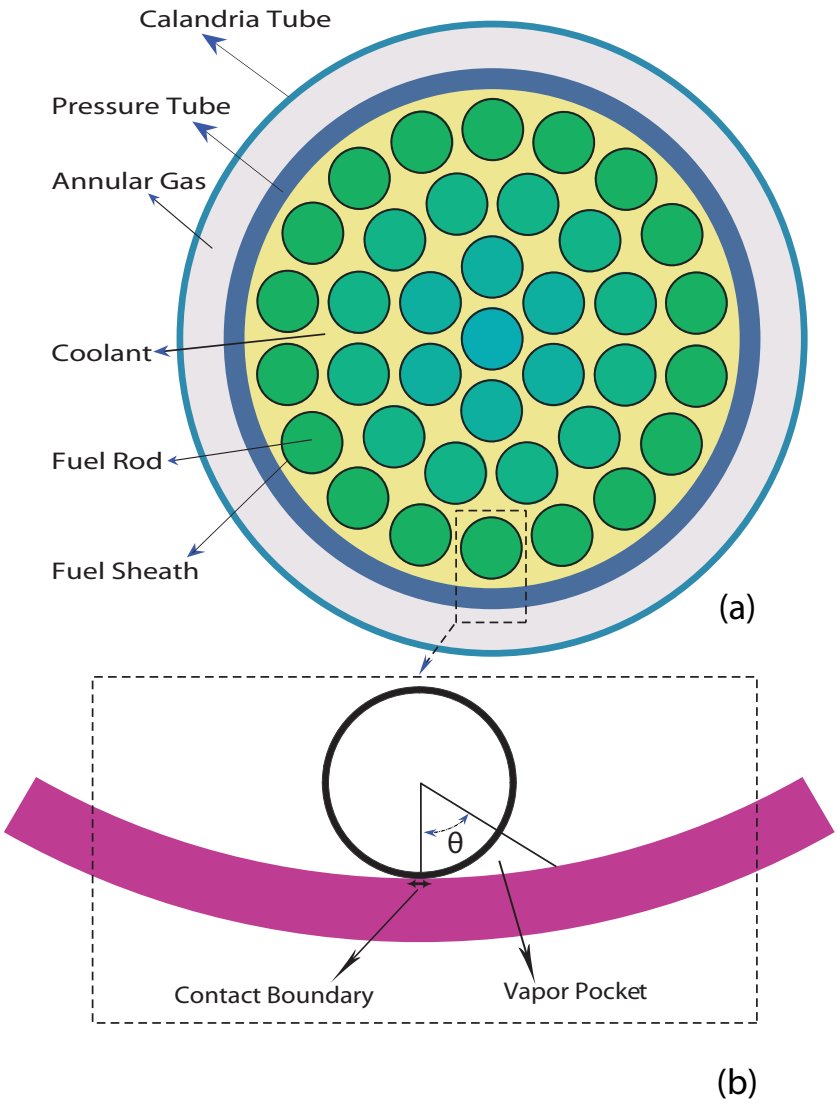

Figure 1. Standard CANDU-6 (a) and when FE/PT contact occurs (b)

detached from the bundle and sits in contact with the pressure tube. This highly unlikely condition is postulated to occur at full power and normal coolant flows and the resulting heat transfer and thermal-mechanical deformation are analyzed to determine the potential consequences of such an event. The contact boundary between the fuel element and pressure tube is considered using the geometry depicted in Figure 1(b). The contact boundary could be either a single spot or a small arc depending on the bundle weight and location.

As a consequence of localized degraded cooling in the region of contact, the coolant could be vaporized on either side of the contact region creating vapor pockets. These vapor pockets might be extended even more (increasing θ) depending on the heat flux of the fuel element and coolant conditions. During such reduction in convective cooling and the extension of vapor pockets if sufficient heat is transferred to the pressure tube through conduction and radiation, then local deformation of the pressure tube may occur. In fact, zircaloy creep strain is sig-

nificantly increased at temperatures greater than approximately 900 K due to α to β phase change.[1,2]

A number of analytical and experimental studies have been performed and published. One of the earlier studies presented by McGee et al.,[3] describes the theoretical models that were made and compared with experimental analysis. The main goal was to evaluate the overall thermal resistance of a joint (consisting of a smooth right circular cylinder in contact with a smooth flat surface). A line contact model was considered to evaluate the thermal resistance of the solid to solid contact (i.e., cylinder to flat contact). For the thermal resistance of the gas-filled gaps on either side of the contact, the decoupled model (DCM), the half-space model (HSM) and the parallel flux-tube model (PFTM) were constructed. These three models differ in the method used to calculate the temperature drop across the joint. Therefore, the total joint resistance was obtained using parallel summation of solid to solid contact with gas-gap thermal resistances. Experimental measurements of the overall thermal resistance were performed in vacuum and with a fluid. Furthermore, the effect of contact pressure was investigated for mechanical loads on specimens fabricated from Keewatin tool steel, stainless steel (type 304) and zircaloy-4. Finally, the authors compared the experimental data with the model predictions and large differences were observed between model and measurement except for a limited range of experimental parameters.

Another study was performed by Reeves et al.,[4] where the authors presented analytical models which predict the transient thermal-mechanical behavior of a pressure tube following the contact of a hot fuel element under loss of coolant accident (LOCA) conditions. The code MINI-SMARTT was developed, based on finite difference techniques to solve the heat conduction equations with radiation and convection to the coolant and contact conduction between any specified number of fuel elements and pressure tube. A ring radiation model has been considered in order to simplify the surface to surface radiation model for the entire 37 fuel elements. This approach produced conservatively high radiation heat fluxes to the region of the pressure tube near the contact point. Using the code NUBALL, creep strain analysis associated with FE/PT contact was performed over a very broad range of calculations and a number of different cases. From the results of sensitivity analysis, the author concluded that the most sensitive parameters relevant to FE/PT contact were the contact conductance, transient time of the contact and contact width.

The MINI-SMARTT code was also used to investigate the effect of bearing pads (BPs) to pressure tube (PT) contact and the code was validated using contact experimental results obtained at AECL-WRL.[5] Zircaloy oxidation at the fuel channel surfaces which drastically decreases the thermal conductivity of any zircaloy components was also considered.[6] They observed that the contact conductance of BP/PT contact was the most important parameter which did not remain constant during heating of the fuel bundle. Contact conductance increased significantly until a threshold temperature was reached and then decreased, once local bulging allowed the pressure tube to deform away from the bearing pad. The authors concluded that contact conductances are small enough to ensure fuel channel integrity when single or multiple bearing pad contacts occur.

Muir et al.,[7] studied the case where the circumferential temperature gradient on the pres-

sure tube is nonuniform resulting a nonuniform hoop stress leading to a nonuniform pressure tube ballooning, which could result in pressure tube failure before occurrence of PT/CT contact. The pressure tube strain rate was calculated using the codes SMARTT and PTSTRAIN. Comparison presented with the code predictions against two different set of experiments which were performed with defected and non-defected pressure tubes at Stern Laboratories and at AECL. The authors explained that although slightly earlier failures were observed for non-defected tubes and slightly later failures were predicted for defected tubes, they could be attributed to the approximations made in the model where the pressure tube was considered as a thin walled tube and remained circular during deformation.

During a postulated LOCA with failure of emergency core injection system (ECIS), if the pressure tube temperature increases sufficiently, the self-weight of the pressure tubes together with the weight of the fuel bundles could cause the pressure tube to sag into contact with the calandria tube. This might be accompanied simultaneously with pressure tube ballooning due to the internal pressure. Therefore, depending on the accident scenarios, other studies were performed either in experimental facilities or with analytical simulations using different computer codes in order to assess fuel channel integrity.[8–12] A very interesting study of complete coolant flow blockage of a single pressure tube in ACR-700 was performed by Gerardi et al.[13] The authors performed several thermal analyses in order to achieve a solid physical framework for the key phenomena of each stage of this accident using the finite element code COSMOSM. During the early stages of this accident the reactor remains at full power and full pressure, resulting in rapid coolant boil off and fuel overheating. Melting of the zircaloy components in the fuel bundle can occur, with relocation of some molten material to the bottom of the pressure tube, and therefore localized bulging of the pressure tube is predicted. According to Muir[7] a 37% reduction in wall thickness of the pressure tube from its initial value results in pressure tube and/or the calandria tube failure. They also concluded that a minimum molten zircaloy mass of about 100 g is required for failure of both the pressure tube and calandria tube.

None of the published papers considered any fuel element to pressure tube contact problem at full power and highly cooling conditions. The present research is focused on establishing the limits for maintaining fuel channel integrity for the situation in which fuel element to pressure tube contact occurs at full power and high coolant flow conditions. Therefore, we have attempted to simulate several analytical contact models which are the simultaneous solutions to the steady state heat transfer and thermal-mechanical equations along with appropriate boundary conditions as a primary analysis for creep strain calculations. Several important key parameters affecting the contact modeling are introduced in order to perform the sensitivity analysis.

2. DESCRIPTION OF THE MODELS

In a CANDU 37 element fuel bundle, four fuel rings containing respectively 1, 6, 12 and 18 fuel elements are considered (see Figure 1(a)). The pitch circle radius of each ring is 0.0 cm, 1.4884 cm, 2.8755 and 4.3305 cm, respectively. The fuel pellet radius is 0.6122 cm and the thickness of the sheath is 0.0418 cm. The inner radius of the pressure tube is 5.1689 cm and its thickness is 0.4343 cm. The gas gap between the pressure and calandria tubes is filled with carbon dioxide and the thickness of gap is 0.8446 cm.[14]

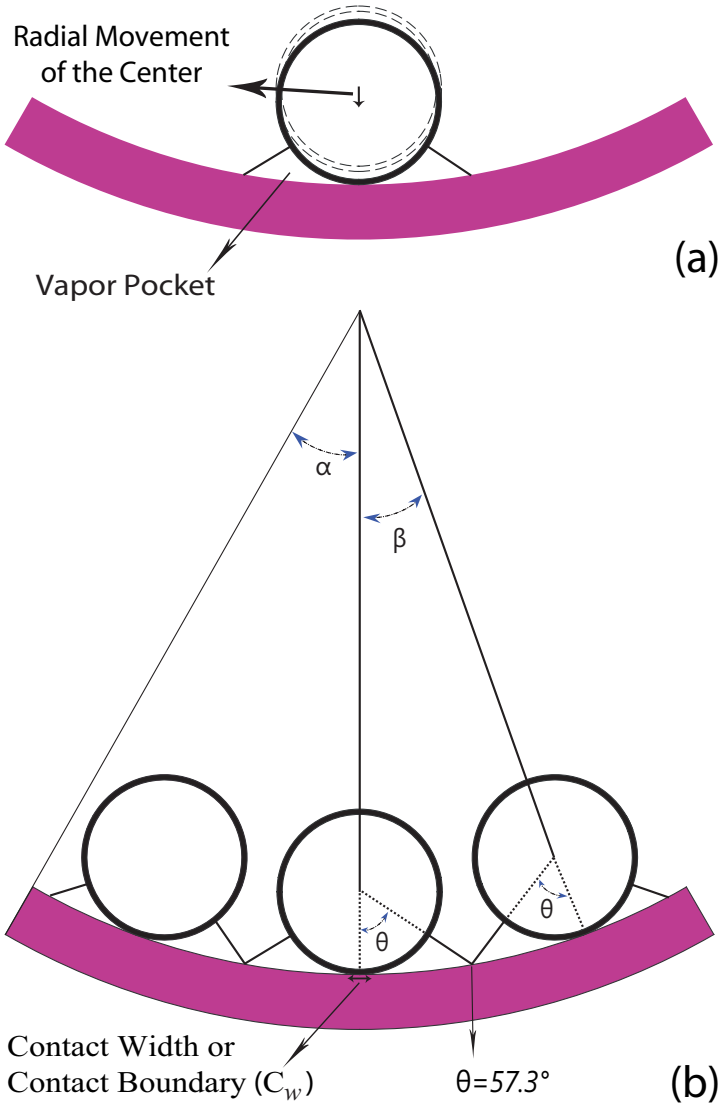

Figure 2. Single FE/PT contact (a) and 3FE/PT contact (b)

Fuel element to pressure tube contact is postulated to occur in a number of different ways. Two different cases are considered here, i.e., single fuel element-pressure tube contact (FE/PT) and a cluster of three fuel elements-pressure tube contact (3FE/PT) (see Figure 2). In the first case, the center of an outer fuel element is displaced radially by 0.1835 cm bringing it into contact with the inner surface of the pressure tube (Figure 2(a)). In the second case, three fuel elements are postulated to radially contact to the pressure tube, in the same way as the first case (Figure 2(b)). Both cases are constructed with a pressure tube arc angle of $2\alpha = 60°$. In the second case, the central locations of the fuel elements are maintained within the same azimuthal step size of $\beta = 20°$.

Coolant is vaporized in the both sides of the contact boundary due to the degraded cooling condition creating local vapor pockets. The extent of the vapor pockets depends on the heat flux of the fuel element and coolant conditions. In order to simulate such conditions, the vapor

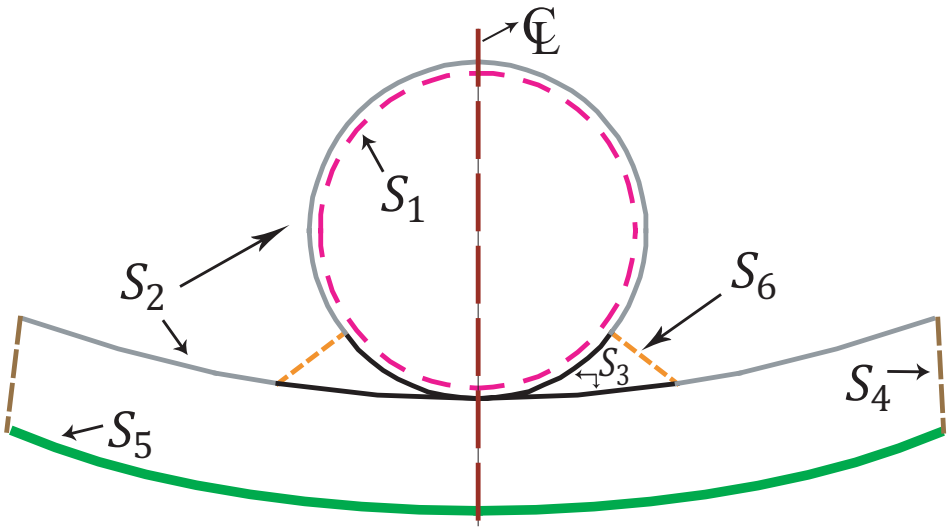

Figure 3. Single FE/PT contact boundaries

pocket dimensions, specified by θ, is uniformly increased in both sides of each fuel element from 15° to 57.3° where they are overlapped according to the Figure 2(b). However, the vapor in these pockets is considered to be stagnated due to the fact that vapor velocity is zero at the boundaries and therefore any motion or convection by vapor is not expected.[15] With regard to radiation heat transfer, a nonparticipating transparent medium is considered inside each vapor pocket that neither absorbs nor scatters the surface radiations and emits no radiation.[15]

The steady state heat transfer equation (1) with appropriate convective and radiation boundary conditions (equation 2,3) are considered for the fuel sheath, pressure tube and transparent vapor pocket regions:

$$\vec{\nabla} \cdot k\vec{\nabla}T = 0 \qquad : \Omega \tag{1}$$

$$\hat{n} \cdot \vec{q''} = \vec{q''_0} + h(T_{wall} - T_\infty) \qquad : S_5 \tag{2}$$

$$(1-\epsilon)R = J - \epsilon\sigma T^4 \Longrightarrow \vec{q''_{rad}} = \epsilon(R - \sigma T^4) \qquad : S_3 \tag{3}$$

where $k(T)$ denotes the thermal conductivity ($\frac{W}{mK}$) as a function of temperature for each domain Ω, i.e., zircaloy-4 fuel sheath, zirconium-2.5% niobium pressure tube and vapor regions which is obtained from the ZRPRO[16] and XSteam-Matlab joint function.[17]

As is shown in Figure 3 only outward fuel element heat flux vector, $\vec{q''_0} = 1.5\ \frac{MW}{m^2}$ is considered on the surface S_1, which is identical to that of $\vec{q'_0} = 60\ \frac{kW}{m}$, a typical high linear rating power of outer elements in a CANDU fuel bundle. On the surface S_5, the heat transfer coefficient $h = 10\ \frac{W}{m^2K}$ has been chosen without consideration of any extra heat sources.[13] The term

$\hat{n}$ is the normal unit vector at each boundary surface and the temperature of the annulus gas gap has been taken as $T_\infty = 180°C$. When vapor pockets are created, radiative heat is transferred through these transparent regions and the inner surface of pressure tube gets hotter and hence, surface to surface radiation boundary conditions must be considered on the S_3 surfaces. The zircaloy emissivity is considered as $\epsilon = 0.8$ and σ is Stefan-Boltzmann constant, R and J are the radiosity and irradiation, respectively. The S_2 surface boundaries are considered to be at fully cooled condition with saturation temperature of coolant, i.e., $T = 310°C$ at 10 MPa pressure.[18,19] On the S_6 surface boundary where the coolant has reached the vapor medium, we have assumed that the evaporation is at the equilibrium with condensation and therefore $T = 310°C$ is implemented. The symmetry boundary conditions are also considered in both ends of the pressure tube S_4.

The pressure tube is under combined internal pressure and radial-circumferential temperature gradient, therefore a nonuniform temperature profile obtained from preceding equations is used to calculate the thermal stress distributions for each domain Ω. In this study only the thermal-elastic deformations of the pressure tube and fuel element are simulated and the yield criterion and the plastic deformation are not considered. The thermal-elastic stresses are obtained from the equilibrium equation (4) and Hook's law (5):[20]

$$\sigma_{ij,i} = -F_j \qquad \sigma_{ij} = \sigma_{ji} \tag{4}$$

$$\sigma_{ij} = \delta_{ij}\lambda(\Theta - 3\alpha T) + 2G(\varepsilon_{ij} - \delta_{ij}\alpha T) \tag{5}$$

$$\Theta = \varepsilon_r + \varepsilon_\theta + \varepsilon_z \qquad \lambda = \frac{\mu E}{(1+\mu)(1-2\mu)} \qquad G = \frac{E}{2(1+\mu)}$$

$$\varepsilon_r = \frac{\partial u_r}{\partial r} \qquad \varepsilon_\theta = \frac{1}{r}\frac{\partial u_\theta}{\partial \theta} + \frac{u_r}{r} \qquad \varepsilon_{r\theta} = \frac{1}{2}\left(\frac{1}{r}\frac{\partial u_r}{\partial \theta} + \frac{\partial u_\theta}{\partial r} - \frac{u_\theta}{r}\right) \tag{6}$$

where σ_{ij} is the stress tensor, $\sigma_{ij,i}$ is a derivative of the stress tensor, F_j denotes the body forces and ε_{ij} is the strain tensor. In fact, we have assumed that a state of plain strain $\varepsilon_z = 0$ is produced where the axial length of pressure tube and fuel element is very large compare to the width of loaded region. Therefore, the strain tensor components are only defined in the two dimensional cases (equation 6) in which (u_r, u_θ) are the radial and circumferential displacements in the cylindrical coordinate and axial displacement is prevented. The term α is the thermal expansion coefficient (K^{-1}), δ_{ij} is the Kronecker delta, μ is the poisson's ratio and $E(T)$ denotes the Young's modulus (Pa) as a function of temperature for each domain. All the material properties are obtained from the ZRPRO. A uniform internal pressure $P_i = 10$ MPa is considered on the S_2 and S_3 surfaces ($\sigma_r \hat{r} \cdot \hat{n} = -P_i$) where the pressure load on the fuel element outer surface will be balanced. An atmospheric pressure $P_o = 101325$ Pa is also considered on the S_5 surface ($\sigma_r \hat{r} \cdot \hat{n} = -P_o$).

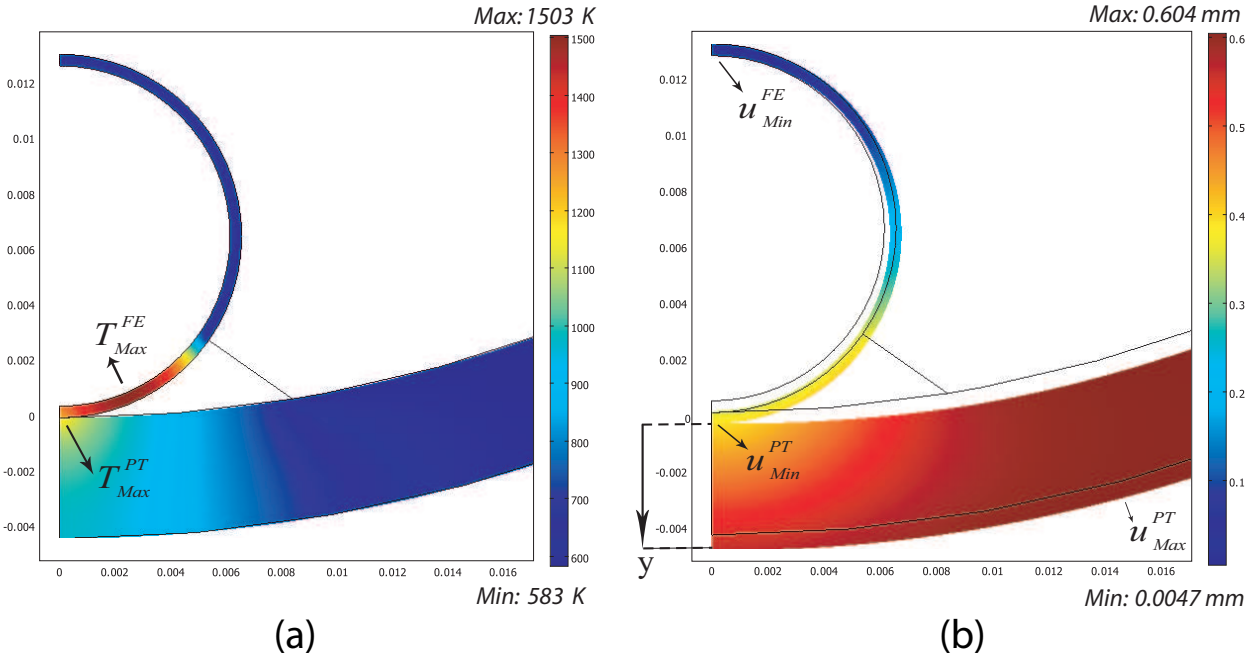

Figure 4. Temperature profile (a) and the total thermal-elastic displacement (b) in FE/PT with spot contact and $\theta = 55°$ vapor pocket.

Based on the principle of virtual work[21] for the total stored energy of system, the above equations and boundary conditions are solved simultaneously with the finite element method[22] in the COMSOL[23] software package. The surface to surface radiation on the boundaries could be calculated either by direct area integration or hemicube method. All these calculations are strongly dependent on the consideration of the contact boundary between the fuel element and pressure tube.[4,24,25] In fact, the pressure which acts on the contacting surfaces and the contact width (C_w) are related to the bundle weight, direction, location and other contact circumstances in the fuel channel. However, the contact boundary could be either a single spot or a small arc. Therefore, the spot model simulation and the arc model simulation performed based on contact boundary.

2.1 SPOT MODEL SIMULATION

In this weightless model, a single spot with perfect contact condition is considered for either the FE/PT or 3FE/PT contact cases. Only a half of domain is simulated due to symmetry in the modeling (see the symmetry line $\mathbb{C}_{\mathbb{L}}$ in Figure 3) . In order to ensure spatial convergence, each domain and boundary must be subdivided into the fine regions. However, for those boundaries where surface to surface radiation condition (S_3 in Figure 3) is considered, even finer mesh element must be chosen. As a result, in the case of FE/PT contact when θ is changed from $15°$ to $57.3°$, the number of mesh and degrees of freedom[22] increased from 6500 and 41300 to 8200 and 47300, respectively. Similarly, in the case of 3FE/PT the number of mesh and degrees of freedom have risen accordingly, from 15500 and 95300 to 20000 and 114200.

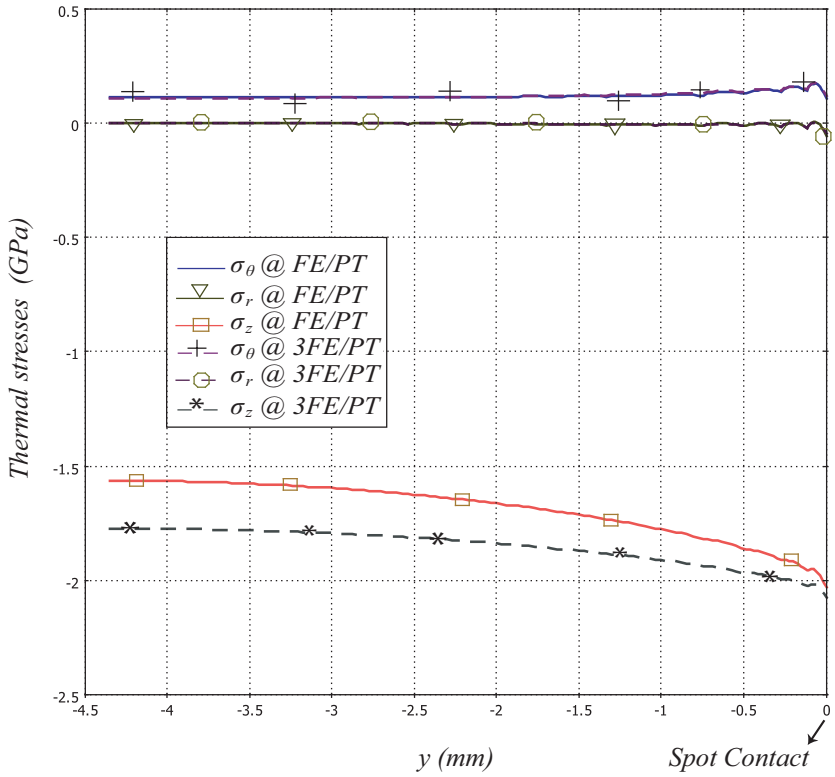

Figure 5. Thermal stresses in FE/PT and 3FE/PT central contact.

Figure 4 (a) shows the solution to the energy equation for the spot contact model (FE/PT case) where $\theta = 55°$. It can be seen that the PT thickness temperature is greater than 900 K where zircaloy creep strain is significantly increased due to α to β phase change. The maximum temperature ($T^{FE}_{Max} = 1503$ K) is obtained in the FE sheath domain while the pressure tube maximum temperature is found to be at spot contact boundary ($T^{PT}_{Max} = 1207$ K). This is because of the fact that heat generated in the fuel pellet could properly transfer into the coolant by convection but partially conducted to the PT through contact point and then transferred through PT thickness to the annulus gas gap. However, those hot regions are achieved due to the lack of proper cooling condition either by conduction, convection and radiation through the vapor pockets. The rest of domain is cooled and temperature remains practically unchanged at 583 K. Although, the maximum temperatures of the FE sheath and PT inner surface are increased when θ increases, however, the behavior of temperature profile obtained for whole domain are pretty similar to that of $\theta = 55°$.

In Figure 4 (b), the total thermal-elastic displacement $\vec{u} = u_r\hat{r} + u_\theta\hat{\theta}$ is shown where we have assumed that the single spot contact is preserved during the thermal-elastic deformation and the outward fuel element heat flux i.e., $\vec{q_0'} = 60\ \frac{kW}{m}$ is fixed on the surface S_1. As a result, the maximum elastic displacement is occurred on the S_5 surface where the PT radius is the highest and the temperature is the lowest i.e., $u^{PT}_{Max} = 0.6$ mm and the minimum deformation i.e., $u^{FE}_{Min} = 0.0047$ mm is obtained on the FE outer surface where is properly cooled by coolant. However, the minimum pressure tube local strain $u^{PT}_{Min} = 0.4$ mm is occurred on the spot contact

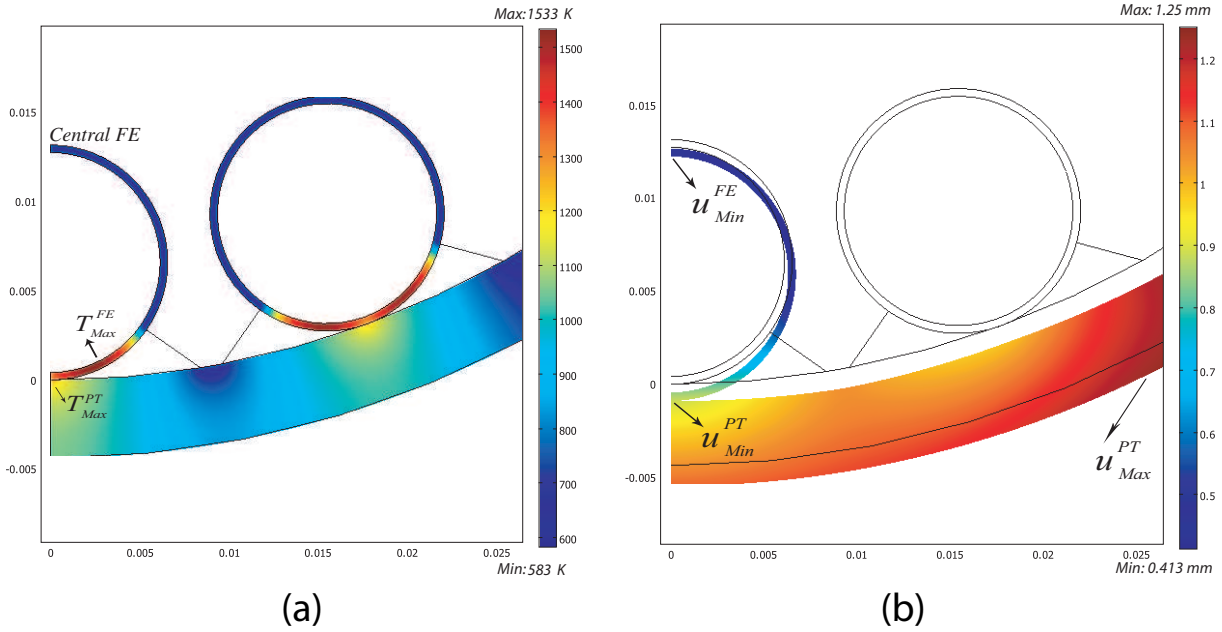

Figure 6. Temperature profile (a) and the total thermal-elastic displacement (b) in 3FE/PT with spot contact and $\theta = 55^{\circ}$ vapor pocket.

boundary where the PT temperature is the highest. In fact, when temperature rises, the pressure tube expands, however, such an expansion generally can not proceed freely in the pressure tube circumferential arc length where the rest of body is maintained at the cooler temperature and acts as a constrain for any expansion. In the other hand, when the thermal stresses are depicted against the radial thickness of the pressure tube (see Figure 5 with y-axis shown in Figure 4 (b)), it can be seen that the radial thermal stress is almost negligible inside the PT thickness, i.e., $\sigma_r \cong 0$ and the tangential (hoop) stress is tensile with a nearly uniform value of $\sigma_\theta = 0.11$ GPa, however, the axial stress is highly compressive within the contact region i.e., $\sigma_z = -2.03$ GPa and decreases toward the PT outer surface i.e., $\sigma_z = -1.56$ GPa, therefore the pressure tube total displacement on the spot contact boundary is lower than that obtained on the S_5 surface.

Figure 6 (a) shows the 3FE/PT contact case with constructed vapor pocket of $\theta = 55^{\circ}$. The maximum temperatures of the central FE sheath (T^{FE}_{Max}) is increased by 30 K and by 17 K in the other fuel sheaths. Accordingly, the pressure tube maximum temperature (T^{PT}_{Max}) is obtained as 1262 K at the central spot contact compare to that of 1237 K at the two other contacts. The total thermal-elastic deformation is also calculated with the same assumptions made on single FE/PT contact case and is depicted in Figure 6 (b). The maximum deformation is obtained on the PT outer surface i.e., 1.25 mm and the minimum on the FE outer surface i.e., 0.413 mm. The minimum PT local strain is occurred on the central spot contact boundary where the PT temperature is the highest i.e., $u^{PT}_{Min} = 0.89$ mm. This result clearly shows the significance of different contact simulations such that when the 3FE/PT contact case has been considered, the pressure tube local strain is increased due to the higher temperature obtained. The thermal stresses are shown in Figure 5. In the 3FE/PT contact case the radial and hoop stresses are almost identical to those obtained in the single FE/PT contact case, and although the axial

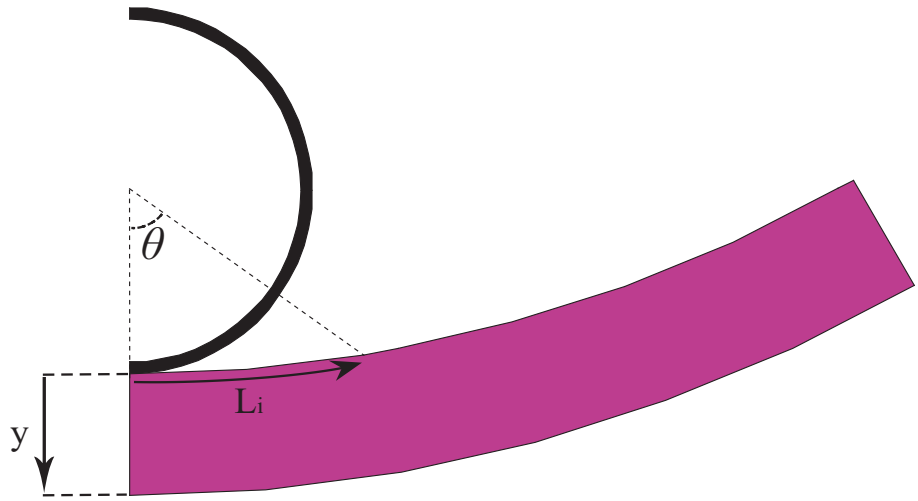

Figure 7. FE/PT contact case: arc length L_i and thickness $\mathbf{y}$.

stress is more compressive, the behavior remains the same as previous one where it is -2.07 GPa compressive on the contact spot boundary and decreases to a value of -1.77 GPa on the PT outer surface.

According to Figure 7, a sensitivity analysis of the PT temperature is performed and depicted in Figures 8 and 9. It can be seen from Figure 8 that the highest temperature of the PT is achieved at the contact point and is decreased across the thickness. However, the PT temperature rises significantly as the vapor pocket dimension increases and hence, after a certain value of θ, i.e., 51° to 57.3° the whole thickness temperature passes the par value of 900 K where considerable creep strain is expected. From Figure 9 it can be seen that the maximum PT temperature increases by 55 K at the central contact compare to that of single FE/PT case. This is mainly due to the reduction of coolant in two parts of pressure tube where vapor pockets are being overlapped, as well as higher heat conduction from two other contact regions. According to Figure 9, the maximum pressure tube temperature increases rapidly even when vapor pocket dimension increases (corresponding to increasing θ) resulting in very little coolant contacting the pressure tube between the fuel elements. These results illustrate the sensitivity of the calculated pressure tube temperature to the assumed coolant boundary conditions.

2.2 ARC MODEL SIMULATION

Although, the weightless spot model has a very good estimation of temperature profiles and local thermal-strain deformations in different contact cases, it can be reasonably assumed that a uniform reaction force develops over the contact area due to the fuel bundle weight. The mechanical deformation of the pressure tube is directly affected by the width of contact between the fuel element and pressure tube. The width of contact is a function of the forces acting on the contacting fuel element, the surface roughness of the interface and the local temperature of the fuel element. Circumferential spreading of contact is not likely to be substantial, as the fuel sheath is supported by ceramic UO_2 pellets, which are not subject to plastic deformation at the

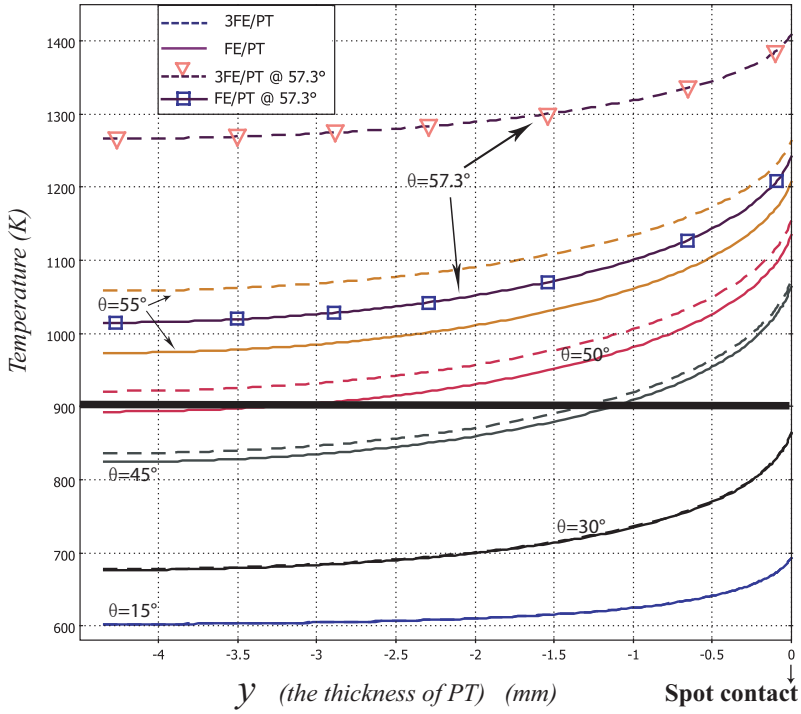

Figure 8. PT temperature profiles with respect to thickness **y**-axis in FE/PT and 3FE/PT central contact cases and vapor development.

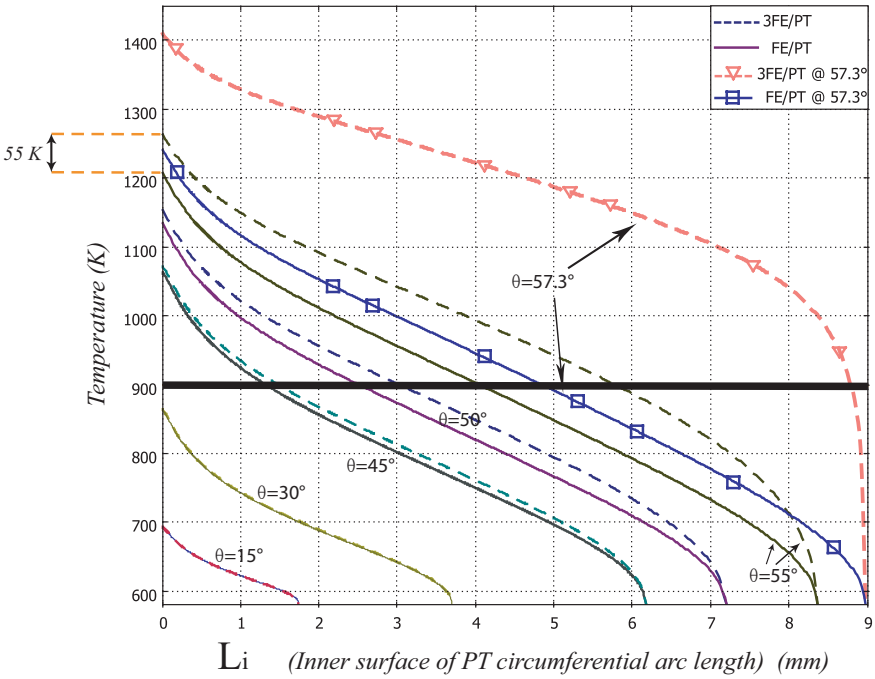

Figure 9. PT temperature profiles with respect to arc length L_i in FE/PT and 3FE/PT central contact cases and vapor development.

temperatures associated with fuel element to pressure tube contact. Based on Hertz theory[25] of elastic contact for cylindrical bodies, Reeves et al.,[4] obtained a width of contact as $C_w = 0.015$ mm for a fuel element at 1273 K contacting a pressure tube at 573 K under 130 $\frac{N}{m}$ uniform lateral FE load. This small value indicates that the introduced spot contact model is initially appropriate, however in those contact scenarios where contact temperature rises and elasto-plastic deformation occurs, the contact width will increase.[24]

The arc model simulation presented here is based on the most sensitive contact parameters i.e., contact width and contact conductance. The simulations are performed for either FE/PT or 3FE/PT contact cases where an extra contact region is also considered between FE and PT. Such a contact boundary region is constructed with a very small uniform thickness of 2 μm according to the zircaloy roughness of fuel sheath and pressure tube.[3] In this study, the contact width and contact conductance are treated parametrically to determine the sensitivity of the pressure tube thermal-mechanical behavior to these parameters. The contact width C_w and contact conductance h are varied between 0.1 mm to 4 mm and 0.5 $\frac{kW}{m^2K}$ to 25 $\frac{kW}{m^2K}$, respectively.[4]

Figure 10 is obtained for the single FE/PT contact case when two different contact conductances i.e., h_5 = 5 $\frac{kW}{m^2K}$ and h_{20} = 20 $\frac{kW}{m^2K}$ are considered in the contact boundary region. The contact length assumed as $C_w = 2$ mm and the vapor pockets are constructed with $\theta = 55^\circ$. The x axis is taken as the inner surface of PT or outer surface of FE circumferential arc length according to S_3 in Figure 3. It is clearly shown that when contact conductance decreases (h_{20} to h_5) or contact resistances increases, the temperature difference between FE and PT significantly increases (120 K to 340 K). However, these results also show that the fuel sheath temperature is more sensitive to h compare to the pressure tube's inner surface temperature. It is interesting to note that this temperature step change could be increased even more when lower contact conductance is considered at the contact boundary region.

Figure 11 shows a temperature profile comparison between single FE/PT contact case with that of obtained for central fuel element at the 3FE/PT contact case. The heat transfer calculations are performed using the contact conductance of h_{20} = 20 $\frac{kW}{m^2K}$ in both cases and a 60 K increase have been achieved in both FE and PT temperature profiles at the contact boundary region. Apparently in this case, the fuel sheath temperature differences are reduced when the circumferential arc length increases while, pressure tube temperature differences are uniformly preserved in the whole vapor pocket. This is mainly due to the consideration of the other two fuel elements as compared to the results obtained with a single FE, in which case more heat energy is conducted to the pressure tube.

In the remaining arc model simulations, a sensitivity analysis has been performed in order to obtain the effect of contact width C_w. In these simulations, once again the vapor pockets are built with $\theta = 55^\circ$ in the FE/PT contact case along with a contact conductance of h_{20} = 20 $\frac{kW}{m^2K}$. It can be seen from Figure 12 that when contact width increases from 0.1 mm to 4 mm the pressure tube temperature reduces almost by 50 K in the center of contact region. However, the temperature profile in the contact boundary is uniformly deceased in the higher contact width, i.e., 1 mm to 4 mm, while it is increased in lower contact width, i.e., 0.1 mm and 0.5 mm. This is due to the fact that when a very small contact width is considered, the heat conduction through the vapor pocket is high and is dominant relative to the contact resistance, therefore,

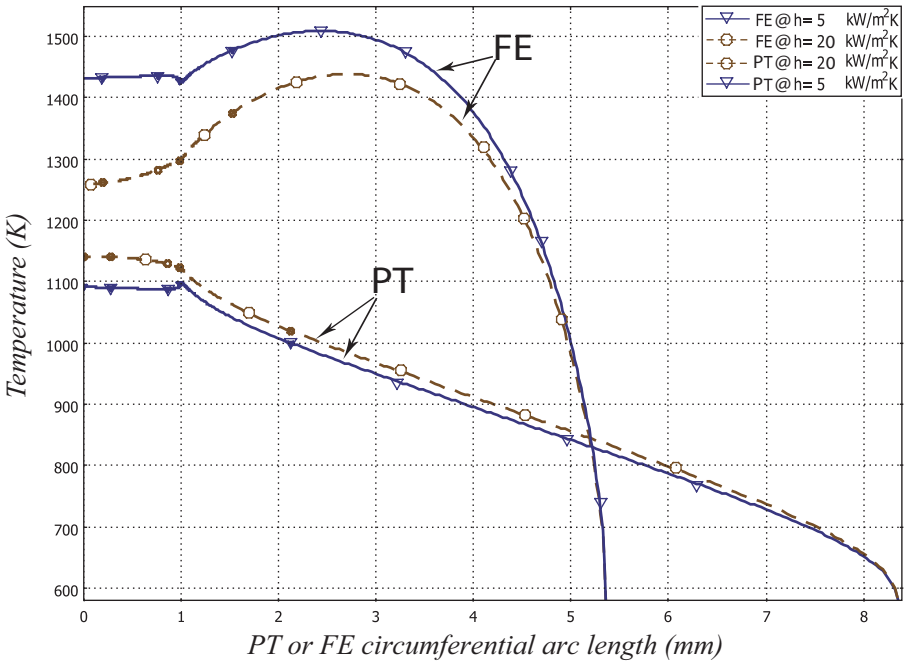

Figure 10. FE/PT temperature profile with different h at $C_w = 2\ mm$ and $\theta = 55°$.

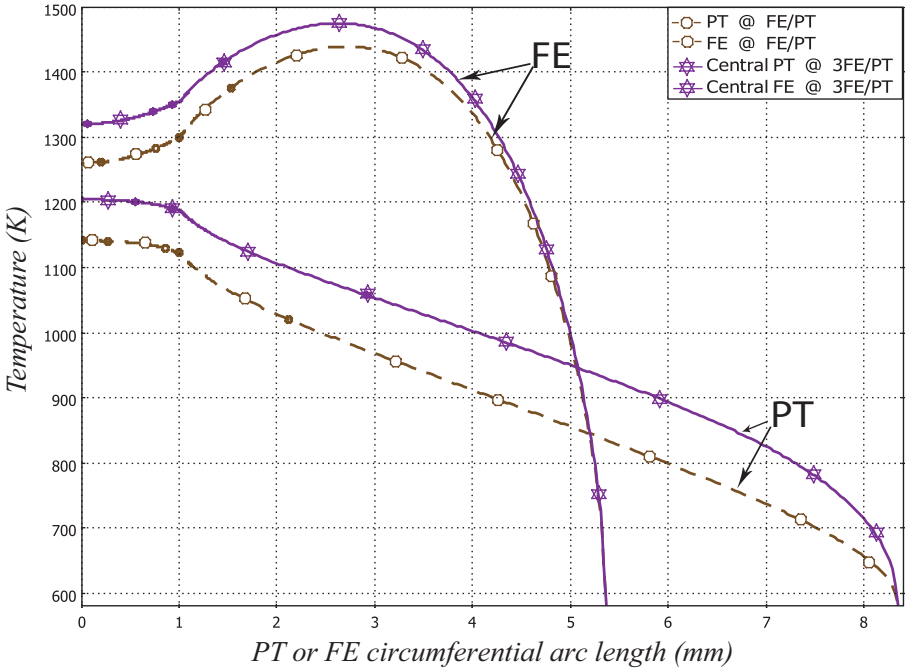

Figure 11. Comparison of FE/PT and 3FE/PT temperature profile at $C_w = 2\ mm$ and $\theta = 55°$.

the pressure tube temperature in the contact edge is increased mostly by vapor conduction and radiation.

The thermal sensitivity of the pressure tube to the contact width C_w is shown in Figure 13 for the 3FE/PT contact case where the vapor pocket dimension θ is uniformly increased in both sides of each fuel element from $15°$ to $55°$ and contact conductance is remained at h_{20} = 20 $\frac{kW}{m^2K}$. It is interesting to note that there is a clear drop in temperature on the inner surface of pressure tube when C_w is increased from $0.1\ mm$ to $4\ mm$. This can be justified by the fact that as the contact width is risen, heat generated in the fuel pellet could properly transfer into the pressure tube through a larger contacting area and therefore conduct to the coolant by the pressure tube thickness, hence, the overall pressure tube temperature is dropped. However, those cases with higher temperature of 900 K and $\theta > 55°$ could experience significant thermal creep strain.

The total thermal-elastic deformation is calculated here in order to compare with those obtained in single spot simulations. The outward fuel element heat flux is assumed to be fixed and the contact width preserved during the thermal-elastic deformation. The 3FE/PT contact case was built with the vapor pocket dimension, $\theta = 55°$, contact width, $C_w = 2\ mm$ and contact conductance, h_{20} = 20 $\frac{kW}{m^2K}$. As a result, the maximum elastic displacement once again is occurred on the S_5 surface where the PT radius is the highest and the temperature is the lowest i.e., $u^{PT}_{Max} = 1.29$ mm and the minimum deformation i.e., $u^{FE}_{Min} = 0.575$ mm is obtained on the FE outer surface where is cooled properly. However, the minimum pressure tube local strain $u^{PT}_{Min} = 0.89$ mm occurs on the contact boundary where the PT temperature is the highest.

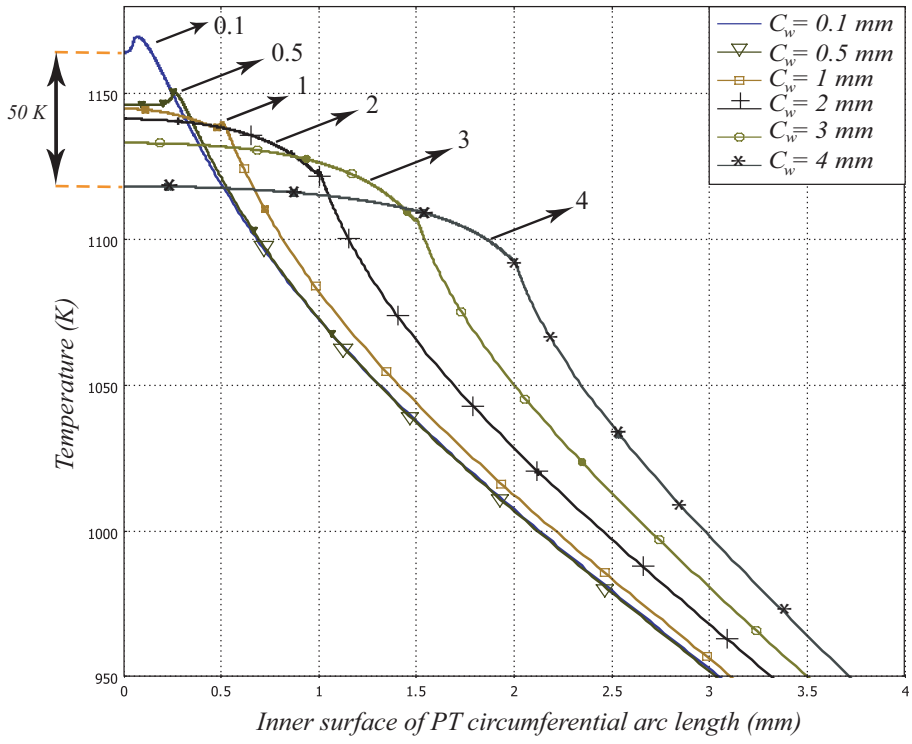

Figure 12. PT temperature profiles in FE/PT contact case with $\theta = 55°$ and different C_w.

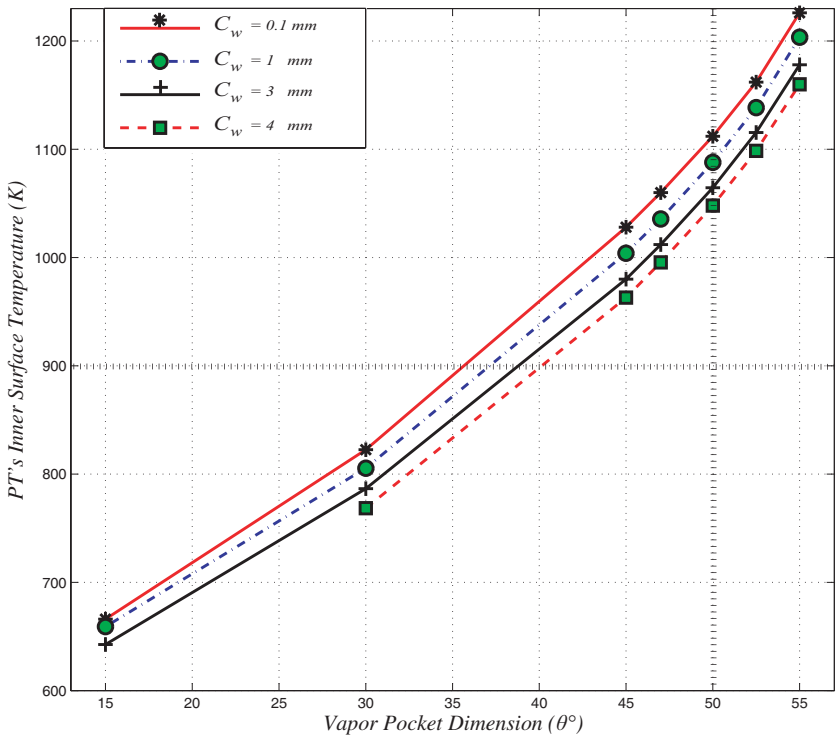

Figure 13. PT's inner surface temperatures in the central contact boundary in 3FE/PT contact case with $h_{20} = 20\ \frac{kW}{m^2K}$ and different C_w.

3. CONCLUSION

Thermal-mechanical behavior of the fuel element to pressure tube contact at full power and highly cooling conditions is considered here in order to investigate potential challenges in fuel channel integrity. We have attempted to simulate several analytical contact models which are the solutions to the steady state heat transfer and thermal-mechanical equations along with appropriate boundary conditions as a primary analysis for the creep strain calculations. The results described here quantify the conditions under which FE/PT or 3FE/PT contact cases could create localized high temperatures on the inner surface of a pressure tube, where the pressure tube local strain occurs. Two different set of simulations have been performed based on contact boundary consideration. The value of parameters considered in these simulations cover a very broad range and many cases. However, the most sensitive parameters which significantly affect the contact modeling are the vapor pocket dimension θ, contact conductance h and contact width C_w. The results demonstrate the strong sensitivity of maximum pressure tube temperature and local strain to the contact conditions and indicate that any local pressure tube deformation will act to reduce the heat transfer to the pressure tube and therefore, will be self-limiting.

ACKNOWLEDGMENTS

Financial support from the Natural Sciences and Engineering Research Council of Canada (NSERC) and the University Network of Excellence in Nuclear Engineering (UNENE) is gratefully acknowledged.

REFERENCES

1. R.S.W. Shewfelt, L.W. Lyall, D.P. Godin, "A High-Temperature Creep Model for Zr-2.5 wt% Nb Pressure Tubes", *Journal of Nuclear Materials*, v 125, i 2, p 228-235, (1984).

2. R.S.W. Shewfelt, L.W. Lyall, "A High-Temperature Longitudinal Strain Rate Equation for Zr-2.5 wt% Nb Pressure Tubes", *Journal of Nuclear Materials*, v 132, i 1, p 41-46, (1985).

3. G.R. McGee, M.H. Schankula, M.M. Yovanovich, "Thermal Resistance of Cylinder-Flat Contacts: Theoretical Analysis and Experimental Verification of a Line-Contact Model", *Nuclear Engineering and Design*, v 86, n 3, p 369-81, (1985).

4. D.B. Reeves, P.S. Kundurpi, G.H. Archinoff, A.P. Muzumdar, K.E. Locke, "Analysis of Fuel Element to Pressure Tube Contact Using the MINI-SMARTT Computer Code", *Proc. 7^{th} CNS Annual Conf.*, p 156-62, (1986).

5. M.H. Bayoumi, W.C. Muir, P.B. Middleton, "Simulation and Analysis of Bearing Pad to Pressure Tube Contact Heat Transfer under Large Break LOCA Conditions", *Proc. 17^{th} CNS Annual Conf.*, Toronto, (1996).

6. V.F. Urbanic, T.R. Heidrick, "High-Temperature Oxidation of Zircaloy-2 and Zircaloy-4 in Steam", *Journal of Nuclear Materials*, 75, p 251-261, (1978).

7. W.C. Muir, M.H. Bayoumi, "Prediction of Pressure Tube Ballooning under Non-Uniform Circumferential Temperature Gradients and High Internal Pressure" ,*Proc. of the 5^{th} Inter. Conf. on Simulation Methods in Nuclear Engineering*, Montreal, (1996).

8. P.M. Mathew, W.C.H. Kupferschmidt, V.G. Snell and M. Bonechi, "CANDU-Specific Severe Core Damage Accident Experiments in Support of Level 2 PSA", *Transactions*, SMiRT 16, Washington DC, (2001).

9. J.C. Luxat, "Mechanistic Modeling of Heat Transfer Processes Governing Pressure Tube to Calandria Tube Contact and Fuel Channel Failure", *Proc. 23^{rd} CNS Annual Conf.*, Toronto, (2002).

10. R.W.L. Fong, C.K. Chow, "High-Temperature Transient Creep Properties of CANDU Pressure Tubes", *Proc. 23^{rd} CNS Annual Conf.*, Toronto, (2002).

11. Yun Jae Kim, Nam Su Huh, Young Jin Kim, Hyun Kyu Jung, "Estimation of Nonlinear Deflection for Cylinder under Bending and its Application to CANDU Pressure Tube Integrity Assessment", *Nuclear Engineering and Design*, v 223, n 3, p 255-62,(2003).

12. P. Majumdar, D. Mukhopadhyay, S.K. Gupta, H.S. Kushwaha, V. Venkat Raj, "Simulation of Pressure Tube Deformation During High Temperature Transients", *International Journal of Pressure Vessels and Piping*, v 81, n 7, p 575-81, (2004).

13. C. Gerardi, J. Buongiorno, "Pressure-Tube and Calandria-Tube Deformation Following a Single-Channel Blockage Event in ACR-700", *Nuclear Engineering and Design*, v 237, n 9, p 943-954, (2007).

14. F. Talebi, G. Marleau, J. Koclas, "A Model for Coolant Void Reactivity Evaluation in Assemblies of CANDU Cells", *Annals of Nuclear Energy*, v 33, n 11-12, p 975-983, (2006).

15. F. Incropera, D. DeWitt, "Introduction to Heat Transfer", second edition, (1990).

16. K.R. Mayoh, "A Compendium of Material Properties for Zirconium Alloys", COG-96-101, (1997).

17. M. Holmgren, "XSteam for MATLAB, Thermodynamic Properties of Water and Steam", http://www.mathworks.com, (2007).

18. S. Glasstone, A. Sesonske, "Nuclear Reactor Engineering", *Krieger Publishing Company*, Malabar, Florida, (1981).

19. N. E. Todreas, M. S. Kazimi, "Nuclear Systems II: Elements of Thermal Hydraulic Design", *Hemisphere Publishing Corporation*, New York, (1990).

20. A. Mendelson, "Plasticity: Theory and Application", *Macmillan*, New York, (1968).

21. S. Timoshenko, J. N. Goodier, "Theory of Elasticity", *McGraw-Hill Book Company*, New York, (1951).

22. O.C. Zienkiewicz, R.L. Taylor, "The Finite Element Method", forth edition, v 2, (1989).

23. COMSOL Heat Transfer Module User's Guide, http://www.comsol.com, (2009).

24. M.M. Yovanovich, "Micro and Macro Hardness Measurements, Correlations, and Contact Models", *Collection of Technical Papers - 44^{th} AIAA Aerospace Sciences Meeting*, v 16, p 11702-11729, (2006).

25. K.L. Johnson, "Contact Mechanics", *Cambridge University Press*, First Published, (1985).